Paper No.
10276

NACE INTERNATIONAL CORROSION 2010 CONFERENCE & EXPO

HIGH SALT CONCENTRATION EFFECTS ON CO_2 CORROSION AND H_2S CORROSION

Haitao Fang, Bruce Brown, Srdjan Nešić
Institute for Corrosion and Multiphase Technology
342 West State Street
Ohio University, Athens, Ohio 45701, USA

ABSTRACT

The general CO_2 corrosion rates of C1018 carbon steel have been measured for NaCl concentrations 3 – 25 wt% at 20ºC, pH 4.0, 5.0 and 6.0. The corrosion process was monitored by linear polarization resistance and potentiodynamic sweeps. AC impedance was used to measure and correct for solution resistance while weight loss was used to verify the corrosion rate magnitude. Experimental results showed that high salt concentrations decreased the general CO_2 corrosion rate significantly and nonlinearly. Potentiodynamic sweep analysis shows that both cathodic and anodic processes were retarded. Flow velocity effects on general CO_2 corrosion rate were minimized due to an increase of salt concentration. No effect of high salt concentration on initiation of localized attack was detected.

A parallel research project was conducted to investigate the high salt concentration effect on H_2S corrosion. The main objective was to study if the high concentration of chloride could initiate localized attack in a H_2S system. Experiments were conducted in a nitrogen purged system with trace amount of H_2S (50 ppm). Weight loss was used to measure corrosion rates. Scanning electron microscopy (SEM), energy dispersive X-ray analysis (EDX) and X-ray diffraction (XRD) methods were used to characterize the morphology, composition and phase identity of the corrosion products. Experimental results show that high salt concentration significantly slowed down the reaction rate in H_2S corrosion. Some pitting attack was found both in salt-free and high-salt conditions. Experimental results did not show evidence that chlorides can initiate localized corrosion in H_2S systems.

Keywords: CO_2 corrosion, carbon steel, linear polarization resistance, potentiodynamic sweep, localized corrosion, chloride, high salt concentration, pitting attack

INTRODUCTION

CO_2 (sweet) corrosion is a complicated process and is affected by many different parameters (for example: temperature, CO_2 partial pressure, pH.), which make it difficult for prediction models to provide accurate results. A large body of research has been conducted in this field over the last three decades. The first significant CO_2 corrosion model introduced by de Waard and Milliams in 1975, identified the combined effect of CO_2 partial pressure and temperature on the corrosion rate as the key parameters in CO_2 corrosion[1]. Since then many other parameters have been uncovered such as pH, velocity, etc[2-7]. However, CO_2 corrosion in solutions with high salt concentrations has not been addressed adequately.

Most previous research related to the effect of salt on CO_2 corrosion focused on the effect of chloride ion concentration in localized corrosion. For example, Sun investigated the effect of Cl^- on localized corrosion in wet gas pipelines[8]. Ma *et al.* also studied the influence of chloride ions on the corrosion of iron[9]. Both investigations concluded that chlorides accelerate localized corrosion. However, the effect of salt content on general CO_2 corrosion was not even mentioned in either paper.

The reality in the field is that dissolved salts (sometimes at very high concentration) are present in water recovered from oil and gas wells. For example a water analysis from a Texas gas well is shown in Table 1. Salt content is about 23 wt% by weight, which is typical for this location. It is not uncommon that salt crystals are seen in the production tubing in Texas, meaning salt concentration could be near saturation. Therefore, it is important to know if this high content of salt has effects on CO_2 corrosion of carbon steel or not.

A series of experiments looking into high salt concentration effects on CO_2 corrosion has been performed and reported for low temperature, 5^oC[10]. A significant salt retardation effect on general CO_2 corrosion rate was observed during those experiments. Adsorption of chlorides was suspected to be the reason for this behavior. The present study was focused on clarifying the salt retardation mechanism by conducting more experiments at room temperature, 20^oC.

The severity of H_2S (sour) corrosion problems in oil and gas production is increasing as fields age and more H_2S is produced. Pitting corrosion along the bottom of the pipeline is the primary corrosion factor leading to failure of sour gas pipelines[11]. It has been suggested that the kinetics of H_2S corrosion is controlled by the nature of corrosion product film, FeS, in terms of both phase type and morphology[12]. Local breakdown of iron sulfide films is suspected to be the main factor in the initiation of localized H_2S corrosion. Breakdown of FeS films may be due to environmental factors, such as the effect of solids, chlorides, sulfur, high velocity[11], etc.

Severe pitting corrosion has been observed in field failures of both wells and pipelines when there were very high concentrations of hydrogen sulfide and chlorides present[13]. However, not many laboratory studies of chloride effect on localized H_2S corrosion have been performed. The role of chloride in localized H_2S corrosion has been insufficiently understood. The present study aimed at filling this gap by conducting H_2S corrosion measurements at high salt concentration (10 wt% NaCl) condition. The ultimate objective is to find out if the high contents of chloride can initiate localized corrosion attack in a low-level H_2S system.

PART 1. HIGH SALT CONCENTRATION EFFECT ON CO_2 CORROSION

EXPERIMENTAL

Specimen Prepararion

The same type of carbon steel (C1018) was used for weight loss, linear polarization resistance (LPR), electrical impedance spectroscopy (EIS) and potentiodynamic sweep analysis. The surface area of the specimen was 5.4 cm^2. The chemical composition of the carbon steel used in the experiment is shown in Table 2Table 3.

The specimen was polished by silicon carbide sand paper before it was tested, and the sand paper grit number used was in the following order: 240, 400, 600. After polishing, the specimen was immersed in isopropyl alcohol in an ultrasonic cleaner for 1 to 2 minutes and then air dried.

Experimental setup

The experiments were performed in a glass cell which is shown in Figure 1. An Ag/AgCl (4M KCl) reference electrode was externally connected to the cell *via* a Luggin capillary with a porous Vycor-tip. A counter electrode was made of a concentric platinum ring. The test matrix for this experimental series is shown in Table 3.

A glass cell was filled with 2 liters of de-ionized water with a desired concentration of NaCl. Cell temperature was followed by a thermocouple. The solution was deoxygenated by purging with CO_2 gas. The solution could be deoxygenated in about 40 minutes to 1 hour of purging. When the desired temperature was attained, the pH of the test solution was adjusted from equilibrium pH to the desired pH by adding a deoxygenated sodium bicarbonate solution. Then a working electrode was put into the solution and all electrical connections were made for corrosion rate monitoring. The rotational speed was set and the open circuit potential was monitored for 20 to 60 minutes for a stable signal before all the electrochemical measurements presented below were carried out.

Measurement techniques

There are two main groups of techniques which were used to monitor the corrosion process. They are electrochemical measurement and weight loss measurement.

The electrochemical measurements were typically conducted in the same order. First, linear polarization resistance (LPR) was performed to measure the corrosion rate, then the solution resistance was measured by conducting electrical impedance spectroscopy (EIS), and last, a potentiodynamic sweep was performed. All electrochemical measurements were made using a Gamry PC4 monitoring system.

The linear polarization resistance (LPR) technique was used to measure the corrosion rate. The steel sample was polarized at ±5 mV or ±10mV around the open circuit potential during the LPR measurement (depending on the level of the inherent electrochemical noise). The scan rate was 0.125 mV/s. What LPR actually measures is polarization resistance, and not corrosion rate. Polarization resistance can be converted to corrosion rate from the basic electrochemical theory. The corrosion current density i_{corr} (A/m^2) is:

$$i_{corr} = B \times \frac{1}{R_p} \times \frac{1}{A} \qquad (1)$$

where, R_p is the polarization resistance as measured by LPR. The solution resistance (R_s) measured by EIS needs to be subtracted from the total corrosion resistance. A is the surface area, which is 5.4 cm^2. B is the 'B value', which can be calculated from the equation below:

$$B = \frac{\beta_a \beta_c}{2.303(\beta_a + \beta_c)} \quad (2)$$

where, β_a and β_c are the anodic and cathodic Tafel slopes, which can be expressed as:

$$\beta_a = \frac{2.303RT}{\alpha_a F} \quad (3)$$

$$\beta_c = \frac{2.303RT}{\alpha_c F} \quad (4)$$

where, T is the absolute temperature in K, R is the universal gas constant (8.314 J/mol K), α_a and α_c are the symmetry factors for anodic and cathodic reactions. The values of α_a and α_c are typically 1.5 and 0.5, respectively. F is Faraday's constant (96,485 C/eq.).

Corrosion rate in mm/yr is then calculated by:

$$CR = \frac{m}{At\rho}\chi = \frac{i_{corr}M_w}{\rho nF}\chi = 1.16 i_{corr} \quad (5)$$

where, m is the metal loss in kg, t is the time in seconds, ρ is the density of the material in kg/m^3, M_w is the molecular weight of iron in kg/mol, n is the number of electrons exchanged in the electrochemical reaction, and χ is the unit conversion factor.

The potentiodynamic sweep technique was used to investigate the corrosion mechanism. The sweeps were conducted with a scan rate of 0.2 mV/s.

Weight loss measurement was used to verify the corrosion rate magnitude. At the same test conditions as electrochemical measurements, a pre-weighed steel sample was put into the test solution. Typically after 24 hours, the sample was taken out of the test solution, rinsed with isopropyl alcohol and wiped with a cloth to remove any salt residue and carbide scales, then air dried and weighed.

RESULTS AND DISCUSSION

Twenty-five glass cell experiments were conducted at 20^{o}C. Some of the tests were repeated several times to check the reproducibility of the results. At the beginning of the experiments, charge transfer control was assumed to be the main corrosion controlling mechanism under these test conditions. Tafel slopes were calculated based on Equations (3) and (4). The B value derived from the equations was B=12 mV.

Figure 2 shows the corrosion rate results measured by LPR and weight loss under the following conditions: pH 4, NaCl: 3 – 20 wt%, 20ºC, flow: stagnant and 1000 rpm. It is apparent that the corrosion rates measured by these two different methods are not in agreement. The weight loss results also show

some flow effect on the corrosion rates. Therefore, the corrosion mechanism apriori assumed for this set of conditions was wrong. As it turned out, the corrosion rate was not under pure charge transfer control but rather under mixed charge/mass transfer control. Therefore, it was difficult to derive explicitly the Tafel slopes βa and βc from potentiodynamic sweeps for this kind of corrosion mechanism. However, the actual B values can be estimated by comparing the polarization resistance measured by LPR and corrosion rates measured by weight loss. Table 4 shows the calculated B values by using this method. The B values shown there are realistic and correspond to a situation when one of the reactions (in this case cathodic) is limited by mass transfer. Figure 3 shows the LPR and weight loss corrosion rates after B value "correction" *i.e.* when the average value B=27 mV/dec is used for all the LPR calculations. As expected the results agree very well.

Test with 3 wt% NaCl

Figure 4 shows the corrosion rate results measured by LPR at 20ºC, pH 4, 1000 and 4000 rpm for a 3 wt% NaCl solution. The LPR corrosion rate is around 2.2 mm/yr at 1000 rpm, and 3.3 mm/yr at 4000 rpm. There is a significant difference in the corrosion rates measured at the lower velocity and the higher velocity under these conditions. Figure 5 shows the potentiodynamic sweep results at different flow velocities. The corrosion potential changed with the flow condition because the cathodic corrosion process is under partial mass transfer control and responded to the increase in velocity.

Test with 10 wt% NaCl

The LPR corrosion rate results are shown in Figure 6 for a 10 wt% NaCl solution. The LPR corrosion rate is around 1.2 mm/yr at 1000 rpm and 1.6 mm/yr at 4000 rpm. Apparently, flow still has an effect on the corrosion rate. A comparison of corrosion rates in 10 wt% NaCl to those in 3 wt% NaCl shows a 50% decrease in the general corrosion rate for all rotational speeds tested, which is similar to the results at 5ºC. Figure 7 shows the potentiodynamic sweep results at different rotational speeds. As was observed at 3 wt%, in the case of 10 wt % NaCl the flow velocity accelerated the corrosion process. But the flow effect seemed to be mitigated by adding more salt.

Test with 20 wt% NaCl

Figure 8 shows the LPR corrosion rate results for a 20 wt% NaCl solution. The corrosion rate is further decreased as compared with the data of 3 wt% and 10 wt% NaCl solutions. Flow velocity effect on LPR corrosion rate continues to become less pronounced. Figure 9 shows the potentiodynamic sweep results. The flow velocity effect on the corrosion process is not significant at this saline concentration, which suggests that the corrosion mechanism gradually changes from mixed charge/mass transfer control to pure charge transfer control with the increase of salt concentration.

Summary of salt effect on the corrosion rate at 20^{o}C

Figure 10 shows the NaCl concentration effect on the LPR corrosion rates. It is seen that NaCl concentration has a significant effect on the corrosion rates. Corrosion rates decrease by 50% as NaCl concentration is increased from 3 wt% to 10 wt%, and decrease further by another 50% as the NaCl concentration is increased from 10 wt% to 20 wt%.

The fact that corrosion rates as measured by LPR decrease with increasing salt concentrations can be explained by looking at potentiodynamic sweep results. Figure 11 and Figure 12 show the cathodic

and anodic curves at different NaCl concentrations at 1000 rpm and 4000 rpm. Independent of the rotational speed, the cathodic curve and the anodic curve show the same trend, both shift to the smaller values as the NaCl concentration is increased. This means that the presence of salt retards both the cathodic and the anodic reaction. This phenomenon is almost identical to what was observed at 5ºC[10]. It should be noted that no initiation of localized attack (pitting) was observed in this series of experiments at any salt concentration.

PART 2. HIGH SALT CONCENTATION EFFECT ON H_2S CORROSION

EXPERIMENTAL

An experimental plan was defined to investigate the high salt concentration effect on H_2S corrosion. Experiments were conducted in salt free D.I. water and at high salt (10 wt%) concentrations. The test matrix is shown in Table 5.

Experimental set-up

The experimental set-up is shown in Figure 13. A cylinder containing mixed nitrogen and approximately 500 ppm H_2S was used as the source of the H_2S. A second cylinder containing pure nitrogen was used to dilute the H_2S concentration from the source by using a mixing gas rotameter. Before the gas was introduced into the test solution, the H_2S concentration in the gas phase was measured with a hydrogen sulfide colorimetric detector tube.

Experiments were performed in a glass cell filled with 2 liters of de-ionized water at a desired salt concentrations (0 or 10 wt%). Initially the test cell was deoxygenated by purging with nitrogen. After that, the hydrogen sulfide gas was introduced and purged continuously. The temperature was controlled by a hot plate with a thermocouple in solution. The pH was adjusted to 5.0 by addition of a deoxygenated hydrochloric acid.

Three sets of specimens were placed into the test solution. A single set of specimens is comprised of 3 specimens. Two specimens were used for weight loss measurement. The third one was used for X-ray diffraction (XRD) analysis. When the first set of specimens was removed after a certain period of time (typically a day), another fresh set of specimens was put back into the test solution, the second set was pulled after a few days, etc. Corrosion product films were analyzed by scanning electron microscopy (SEM), energy dispersive X-ray analysis (EDX) and XRD. Corrosion products were then removed by treatment with Clarke's solution (ASTM standard G1 section 7.7.2 approved by ASTM committee, April 24, 1981) and then corrosion coupons were recharacterized by SEM.

Specimen preparation

The same type of carbon steel (C1018) was used in all the experiments. Specimens were polished with silicon carbide sand paper prior to being tested. The 240, 400, 600 grit sand paper was used sequentially. After polishing, specimens were immersed in an ultrasonic cleaner with isopropyl alcohol for 1 to 2 minutes, and then air dried.

EXPERIMENTAL RESULTS AND DISCUSSION

Tests in DI-water

H_2S corrosion experiments were first performed in a salt-free condition. The purpose of this experiment was to determine whether localized corrosion could be initiated in the absence of chlorides i.e. when carbon steel specimens have been exposed only to an H_2S environment for an extended period of time.

Figure 14 shows the change in corrosion rate with time. The low corrosion rates observed suggest that an iron sulfide film formed immediately on the metal surface and gave protection. Figure 15 shows the pH and iron concentration change with time. The pH increased significantly from 5 to 7 after one day then remained stable at around 7. The dissolved ferrous iron concentration in the solution was measured at around 1ppm. This suggests that most of the dissolved iron generated by the corrosion process was converted to an iron sulfide film.

Surface Analysis after Different Exposure Times

1 day

A SEM picture of the bare metal before exposure is shown in Figure 16 in order to enable comparisons with the surface morphology of corrosion specimens after experiment. Figure 17 shows the SEM image and EDX spectrum of a specimen surface after a 1 day exposure. A very thin layer was formed on the specimen surface. The film appears to be fragmented. EDX data show that sulfur and iron are the main components of the films, consistent with the formation of iron sulfide.

4 days

Figure 18 shows the morphology of the iron sulfide film formed on the specimen surface after 4 days of exposure to H_2S. Compared with the 1 day result, the iron sulfide film at 4 days appears to be thicker. However, the film is still sufficiently thin that the polishing marks can be readily observed. Iron sulfide film was removed by a Clarke solution. The final surface morphology is shown in Figure 19. EDX analysis confirmed that the iron sulfide film had been removed from the surface. No initiation of localized corrosion was observed under this condition.

6 days

After 6 days exposure to H_2S, iron sulfide film became much thicker (Figure 20). A new feature can be observed: iron sulfide "blooms" which formed on top of the more-or-less uniform iron sulfide film. EDX analysis shows that the sulfide content of the bloom is much higher than that of the uniform sulfide film; however, this could be an artifact related to the EDX technique. SEM image of the specimen surface after film removal is shown in Figure 21. At several points what appears to be pitting attack was observed on the metal surface. The diameter of these small pits varied from 6μm to 15 μm. A 3D software reconstruction of SEM images was used to analyze the pit depth. Figure 22 shows the 3D view of one such pit. The pit depth is around 40 μm so the corresponding time-averaged pitting rate is calculated to be around 2.4 mm/yr. Compared with the general corrosion rate of 0.017 mm/yr, the localized corrosion rate is at least two orders of magnitude higher.

12 days

The iron sulfide film kept growing with time. Iron sulfide "blooms" formed on the metal surface in greater quantity (Figure 23). The composition of the iron sulfide "bloom" at 12 days was similar to the one at 6 days. After film removal at 12 days exposure, pitting corrosion was again observed. The

pitting density at 12 days was higher than that seen at 6 days (Figure 24). More and more small pits were observed after the corrosion product was removed by Clarke solution. The deepest pit depth observed is around 14μm (Figure 25) suggesting that the pit size change was not happening over time, i.e. no pit propagation was detected.

Why Did Pitting Attack Initiate and Not Propagate?

As stated above, some pitting (localized corrosion) was observed on the specimen surface even in the salt-free test conditions. Exposed specimens were re-examined by SEM and EDX to try to establish the reason of pitting initiation. Figure 26 shows one location of the specimen surface without the iron sulfide films at 6 days exposure to a salt-free solution at 25°C, showing what appears to be a bead of a different material at the bottom. EDX results confirmed the presence of aluminum and magnesium inside the pits. It is suspected that these may have been present as inclusions in the parent steel or were introduced by the surface polishing process. The feasibility of the first assumption was confirmed by looking at steel composition and consulting the steel maker. The latter needed further investigation. Figure 27 shows the surface of a bare metal surface polished by sand paper: aluminum and magnesium were also found. Gold coated sand paper was further analyzed by EDX and the same elements were found (Figure 28) confirming that the metal inclusion in the steel may have been related to specimen preparation.

It can be concluded that pitting was initiated due to the presence of the inclusions in the steel surface. Once the steel around the inclusions was dissolved away sufficiently, the inclusions were removed and pit propagation stopped.

10 wt% NaCl

In the second series of experiments, the salt concentration was increased to 10 wt% in order to investigate the effect of high chloride concentrations on localized H_2S corrosion of carbon steel. Similar pitting corrosion attack was also observed in the high salt conditions as was seen at salt-free conditions described above. However, the higher salt concentration significantly decreased the uniform corrosion rate (Figure 29) as well as the pitting corrosion.

Surface Analysis after Different Exposure Times

1 day

Figure 30 shows the SEM image of the specimen surface after 1 day exposure to H_2S at 10 wt% NaCl, 25°C. There is barely any iron sulfide film formed on the metal surface in comparison to similar observations in salt-free conditions. The high salt concentration also significantly retarded the uniform corrosion rate as measured by weight loss. A significant quantity of sodium chloride is observed in the SEM, crystallized on the metal surface due to rapid dehydration of the specimen by alcohol upon retrieval from the glass cell.

3 days

In this case the corrosion specimen was first rinsed with a deoxygenated DI water to remove sodium chloride after retrieval from the glass cell, therefore, no NaCl crystals were observed on the specimen surface. Thicker iron sulfide film was observed after the corrosion specimen was exposed to H_2S for 3 days (Figure 31). However, the FeS film was not uniform.

7 days

Blooms in the iron sulfide film appeared on the specimen surface (Figure 32), which are more concentrated when compared with the films observed at 7 days in salt-free conditions. However, the rest of the film is relatively thin. The general corrosion rate at high salt concentration condition is still very low. Some pitting attack was evident after the film was removed by Clarke solution (Figure 33). However, the pits were too small to quantify in depth.

15 days

The morphology of iron sulfide films at 15 days was similar to the film morphology observed at 7 days (Figure 34). The difference is that the iron sulfide film at 15 days was visibly thicker as suggested by the SEM image. Figure 35 shows the SEM image of the specimen surface without iron sulfide films at 15 days. Some pitting attack was observed, a 3D analysis of the pit is shown in Figure 36.

26 days

Figure 37 shows the iron sulfide film morphology after the corrosion specimen was exposed to H_2S for 26 days. Some major cracks of the iron sulfide films were observed. Large and deep pits were expected; however, no severe pitting corrosion was observed after the iron sulfide film was removed.

High salt concentration effect

According to the experimental results shown above, it appears that high salt concentrations significantly retarded the overall general corrosion reaction rate of mild steel in the presence of small amount of H_2S. Figure 38 shows the comparison of localized and general corrosion rates with different salt concentrations at 25^{o}C, 50 ppm H_2S, after 12 days. Results show that an increase in the salt concentration decreased both the general corrosion rate and the localized corrosion rate under these conditions. Pitting corrosion initiation was observed in both salt-free and high salt concentration conditions, however no propagation of pits was seen. Steel inclusions and other imperfections were expected to have caused the initiation of localized attack to the carbon steel in this series of experiments. Therefore, the initial hypothesis that chlorides would initiate and lead to severe localized corrosion (pitting) in a low-level H_2S environment was not confirmed by these experiments. Clearly more research is needed to look at higher H_2S concentrations, higher temperatures, complicating effects of CO_2, etc.

CONCLUSIONS

- The CO_2 general corrosion rate of carbon steel significantly decreases with the increase of salt concentration.
- With the increase of salt concentration, the general CO_2 corrosion mechanism gradually changes from mixed charge transfer/limiting current control to a higher degree of charge transfer control
- In general CO_2 corrosion, an increase in salt concentration retards the heterogeneous charge transfer reactions, as well as the homogenous chemical reactions and mass transfer processes.
- In the low level H_2S system, initiation of pitting corrosion was observed under both salt-free and high salt concentration conditions. However, no pitting propagation was seen in either case.
- Higher temperature, higher H_2S concentration and complicating effects of CO_2 need to be considered in the future study.

- A high salt concentration significantly retarded the uniform corrosion rate in the H_2S system investigated.

REFERENCES

1. C. de Waard, D.E. Milliams, "Carbonic Acid Corrosion of Steel", Corrosion, Vol 31, Paper no. 5, 1975, p177.

2. C. de Waard and D.E Milliams, "Predictive Model for CO_2 Corrosion Engineering in Wet Natural Gas Pipelines", Corrosion/91, Paper No.577, NACE International.

3. C. de Waard, U.Lotz, "Prediction of CO_2 Corrosion of Carbon Steel," Corrosion/93, Paper no. 69, NACE International, Houston, Texas, 1993.

4. C. de Waard, U.Lotz, A.Dugstad "Influence of Liquid Flow Velocity on CO_2 Corrosion: A Semi-empirical Model". Corrosion/95, Paper no. 128, NACE International, Houston, Texas, 1995.

5. Linda D.S. Gray, Bruce G. Anderson, Michael J. Danysh, and Peter R. Tremaine, "Mechanisms of Carbon steel Corrosion in Brines Containing Dissolved Carbon Dioxide at pH 4", Corrosion/89, Paper no. 464, NACE International, Houston, Texas, 1989.

6. L. D.S. Gray, B. G. Anderson, M. J. Danysh, and P. R. Tremaine, "Effect of pH and Temperature on the Mechanisms of Carbon steel Corrosion by Aqueous Carbon Dioxide", Corrosion/90, Paper no. 40, NACE International, Houston, Texas, 1990.

7. S. Nesic, J. Postlethwaite, and S. Olsen "An Electrochemical Model for Prediction of Corrosion of Mild Steel in Aqueous Carbon Dioxide Solutions", Corrosion 2003, 52, P.280.

8. Y. Sun, K. George, S. Nesic "The Effect of Cl^- and Acetic Acid on Localized CO_2 Corrosion in Wet Gas Flow", Corrosion/2003. Paper no. 03327, NACE International, Houston, Texas, 2003.

9. H. Ma, C. Yang, G.Li, W. Guo, S. Chen, J. Luo "Influence of nitrate and chloride ions on the corrosion of iron", Corrosion 2003, 59, P.1112.

10. H. Fang, Srdjan Nesic, B. Brown and S. Wang "General CO_2 Corrosion in High Salinity Brines", Corrosion/06, Paper no.06372, NACE International, Houston, Texas, 2006.

11. Technical Document, "Recommended practice for mitigation of internal corrosion in sour gas gathering systems", Canadian Association of Petroleum Producers. January, 2003.

12. T.W. Hamby, “Development of High Pressure Sour Gas Technology”, JPT, p. 792, 1981.

13. Ho-Chung-Qui, D.F and A.I. Williamson, “Corrosion Experiences and Inhibition Practices in Wet Sour Gas Gathering Systems, Corrosion/87, Paper No. 46, NACE 1987.

TABLES

Table 1. A water analysis summary for a Texan gas well

Compound	Compound (mg/l)	Concentration wt.%
NaCl	131080	13.1
$CaCl_2 \cdot 2H_2O$	111510	8.36
$MgCl_2 \cdot 6H_2O$	50810	2.39
TOTAL	293400	23.85

Table 2. Chemical composition of C1018 carbon steel (wt%)

C	Si	P	S	Mn	Al	Fe
0.21	0.38	0.09	0.05	0.05	0.01	balance

Table 3. Test Matrix for CO_2 Experiments

Parameters	**Conditions**
Total Pressure	1bar
Temperature	20 ºC
Rotation Speed	1000, 4000 rpm
NaCl Solution	3, 10, 20, 25 wt%
pH	4.00
Material	C1018

Table 4. B value calculations at pH 4, 20ºC

NaCl concentration	Weight Loss	Rp	Area	B	$B_{average}$
wt.%	mm/yr	ohms	cm^2	mV/dec	mV/dec
3	2	26.2	5.4	24	27
10	1.46	48.9	5.4	33	
20	0.46	110.8	5.4	24	

Table 5. Test Matrix for H_2S Experiments

Parameters	Conditions
Total Pressure	1bar
H_2S concentration	50ppm
Temperature	25ºC
NaCl Solution	0 wt%, 10 wt%
pH	5.0
Material	C1018

FIGURES

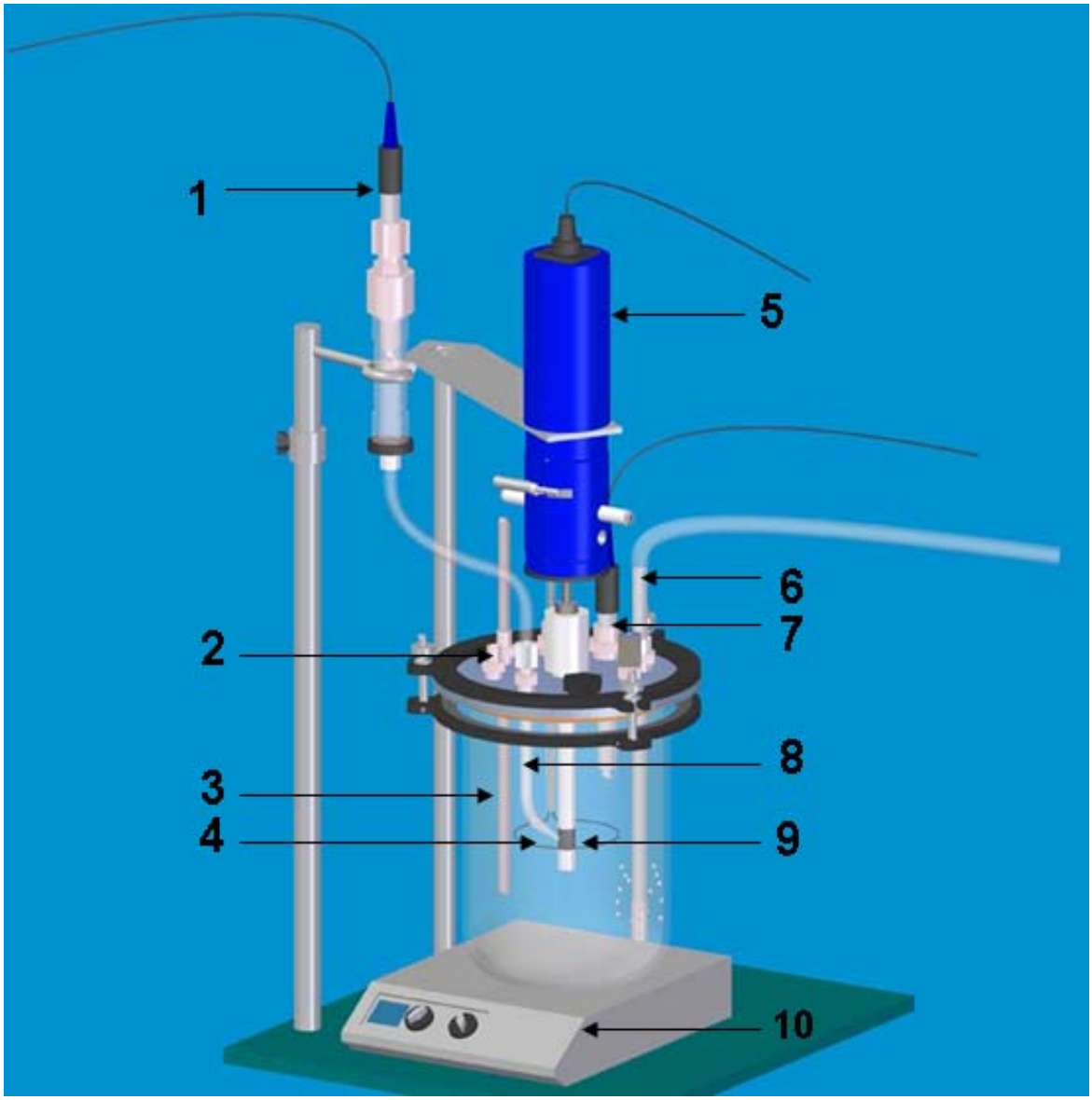

1. Reference electrode
2. Gas outlet
3. Temperature probe
4. Platinum counter electrode
5. Rotator
6. Gas inlet
7. pH-electrode
8. Luggin capillary
9. Working electrode
10. Hot Plate

Figure 1. Schematic of a glass cell for CO_2 corrosion

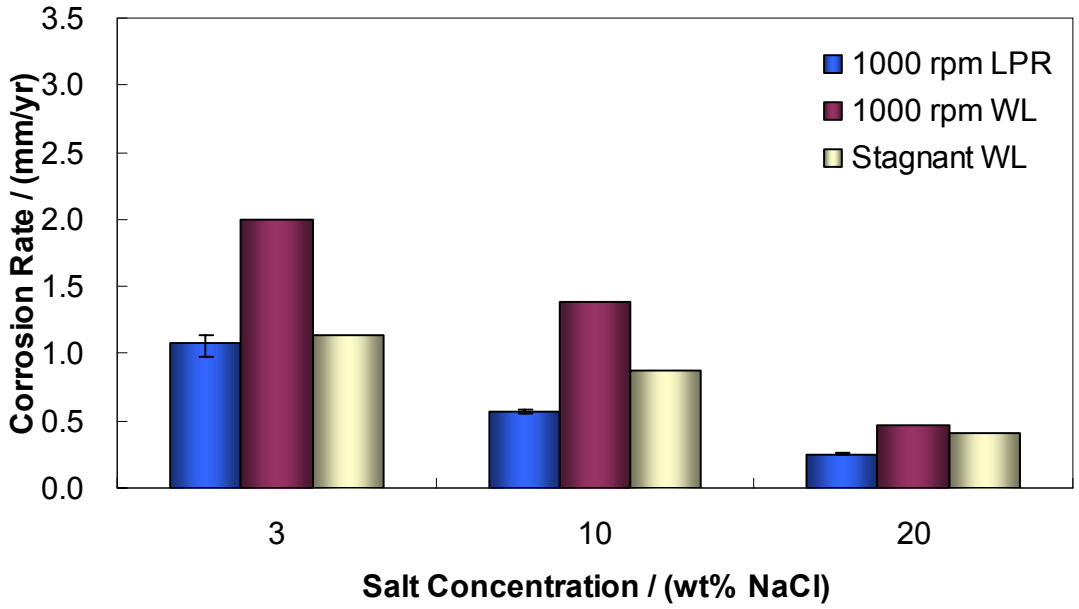

Figure 2. LPR and weight loss corrosion rates in CO_2 purged solutions (20ºC, pH 4, 3 wt%, 10 wt%, 20 wt% NaCl, B=12 mV/dec)

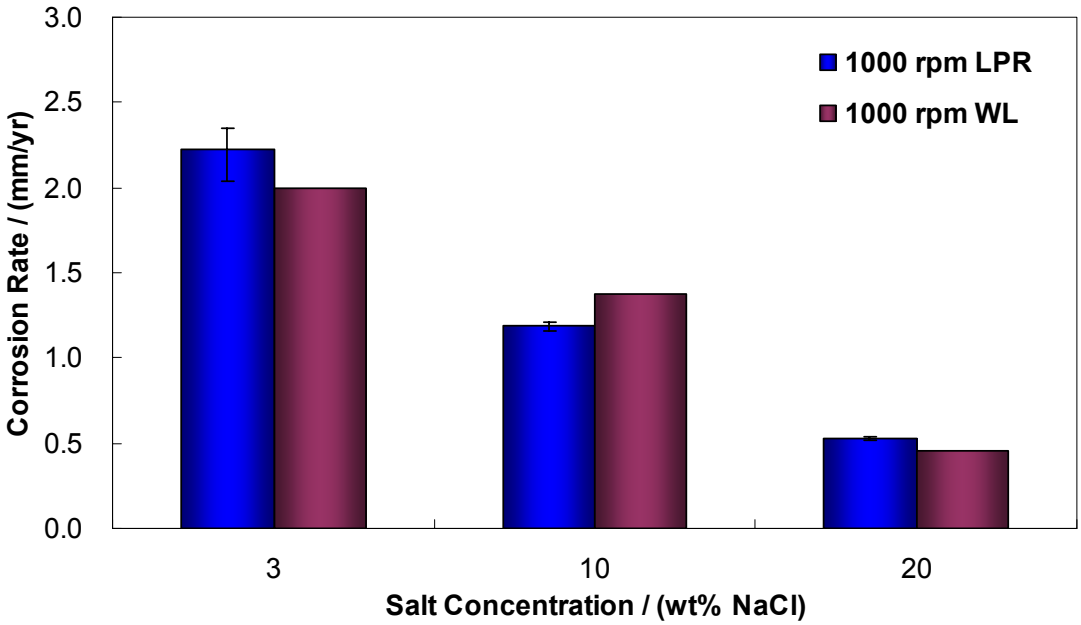

Figure 3. LPR(corrected B value) and weight loss corrosion rates in CO_2 purged solutions (20ºC, pH 4, 3 wt%, 10 wt%, 20 wt% NaCl， B=27 mV/dec)

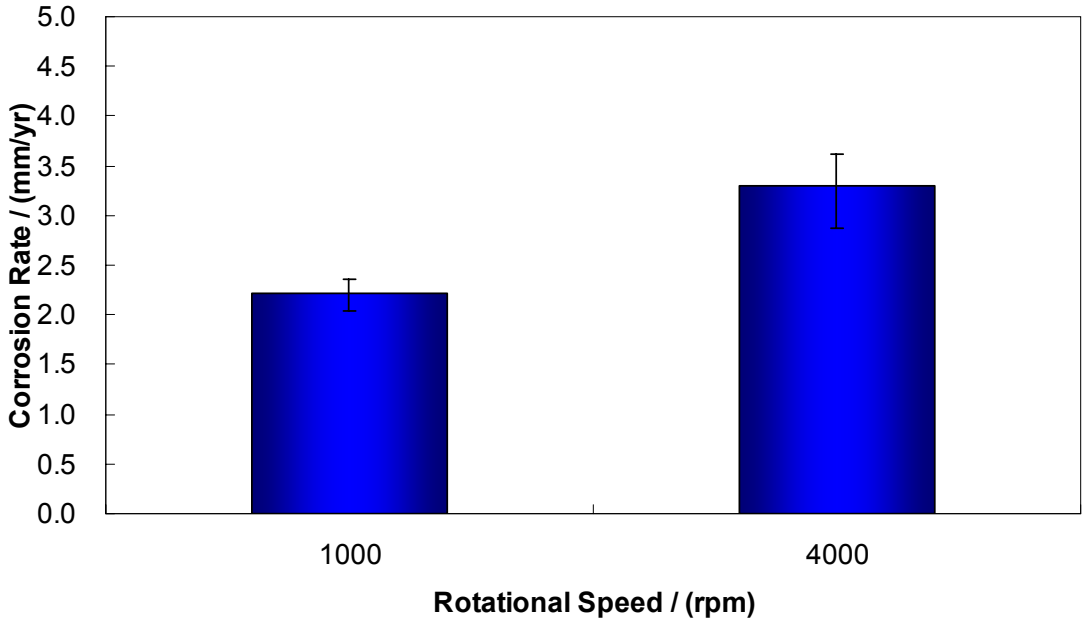

Figure 4. Flow velocity effect on LPR corrosion rate in CO_2 purged solutions (1000 – 4000 rpm, pH 4, 3 wt% NaCl, 20ºC)

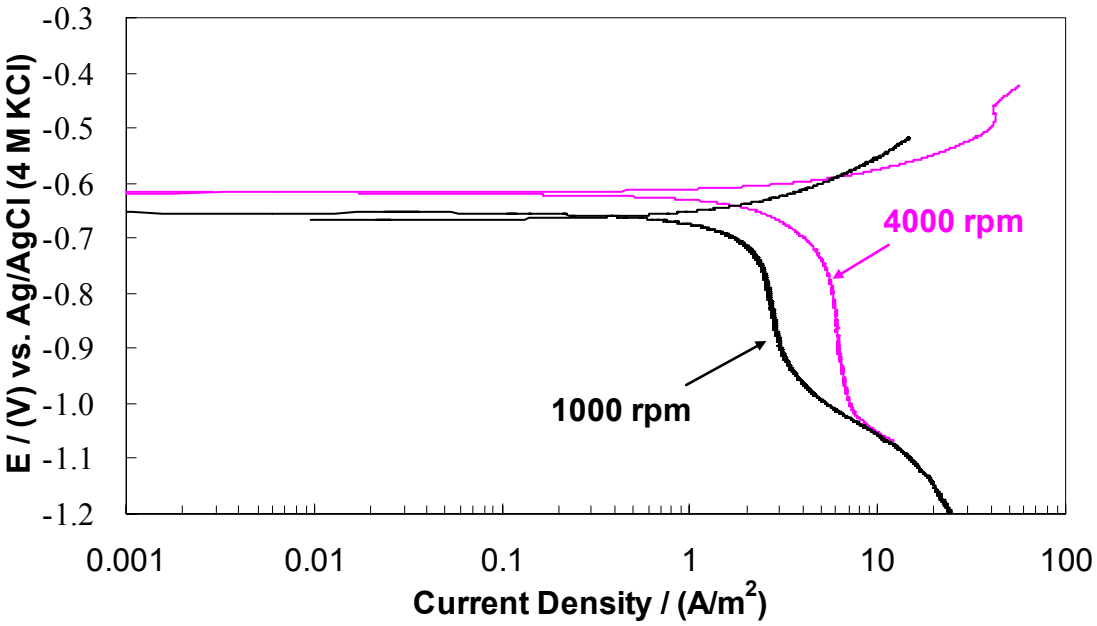

Figure 5. Flow velocity effect on potentiodynamic sweep in CO_2 purged solutions (1000 – 4000 rpm, pH 4, 3 wt% NaCl, 20ºC)

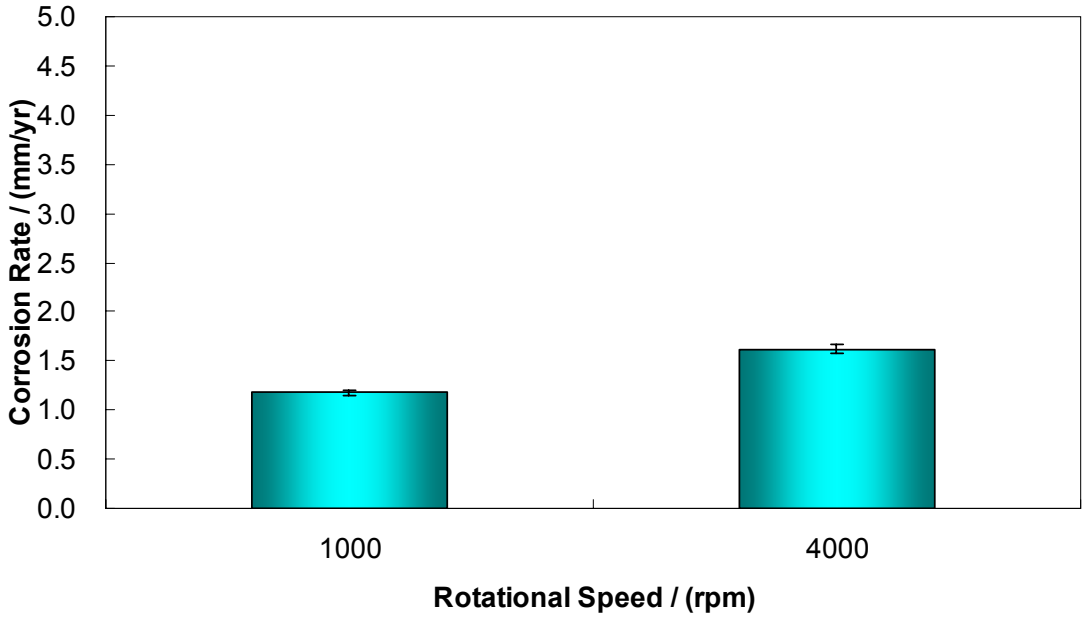

Figure 6. Flow velocity effect on LPR corrosion rate in CO_2 purged solutions (1000 – 4000 rpm, pH 4, 10 wt% NaCl, 20ºC)

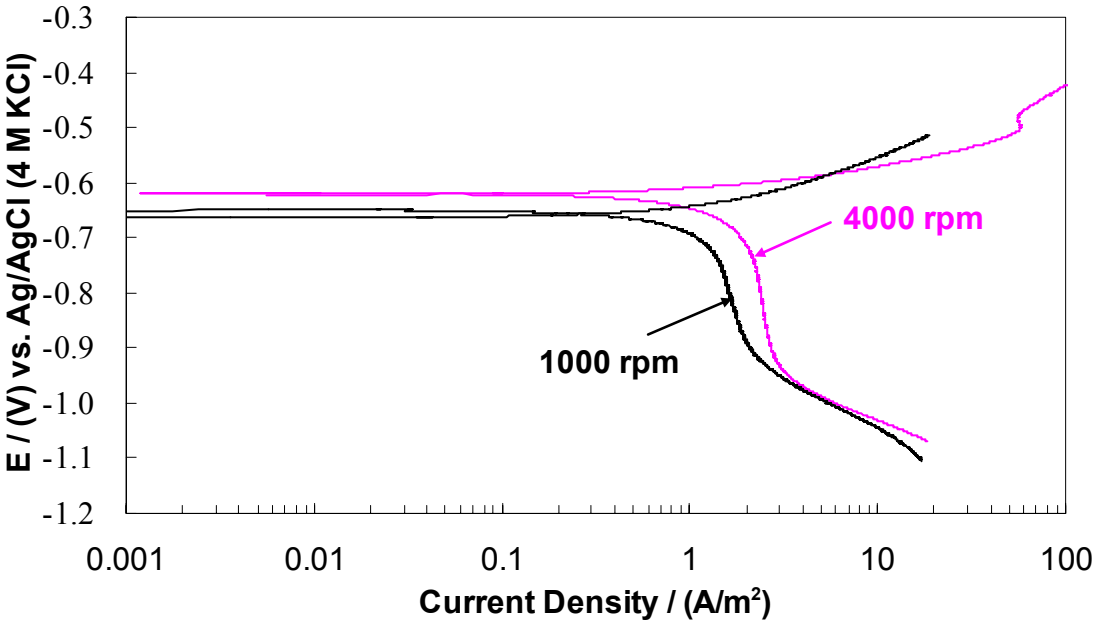

Figure 7. Flow velocity effect on potentiodynamic sweep in CO_2 purged solutions (1000 – 4000 rpm, pH 4, 10 wt% NaCl, 20ºC)

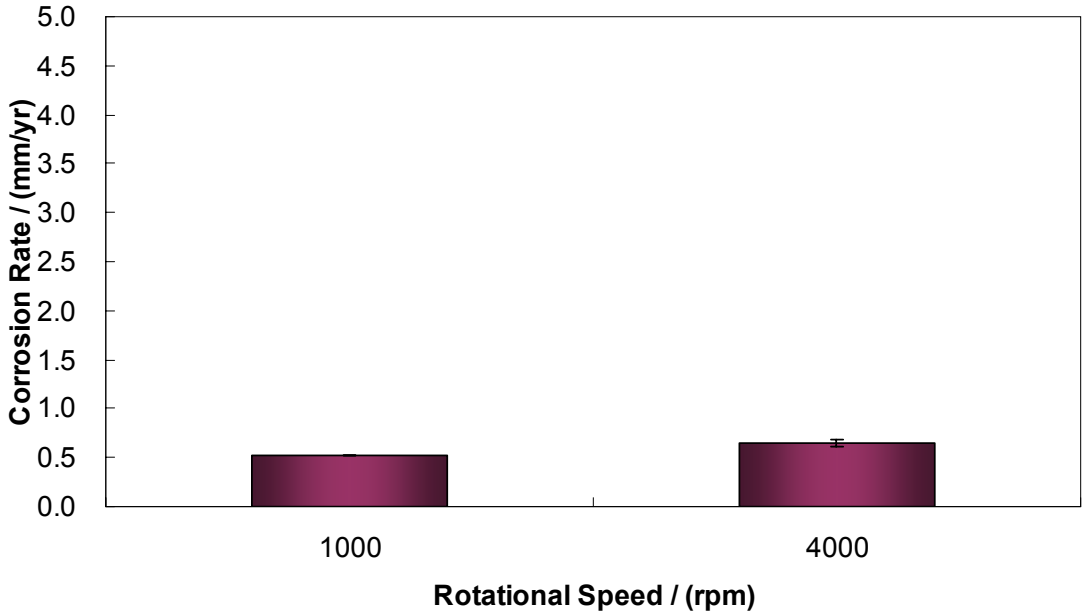

Figure 8. Flow velocity effect on LPR corrosion rate in CO_2 purged solutions (1000 – 4000 rpm, pH 4, 20 wt% NaCl, 20ºC)

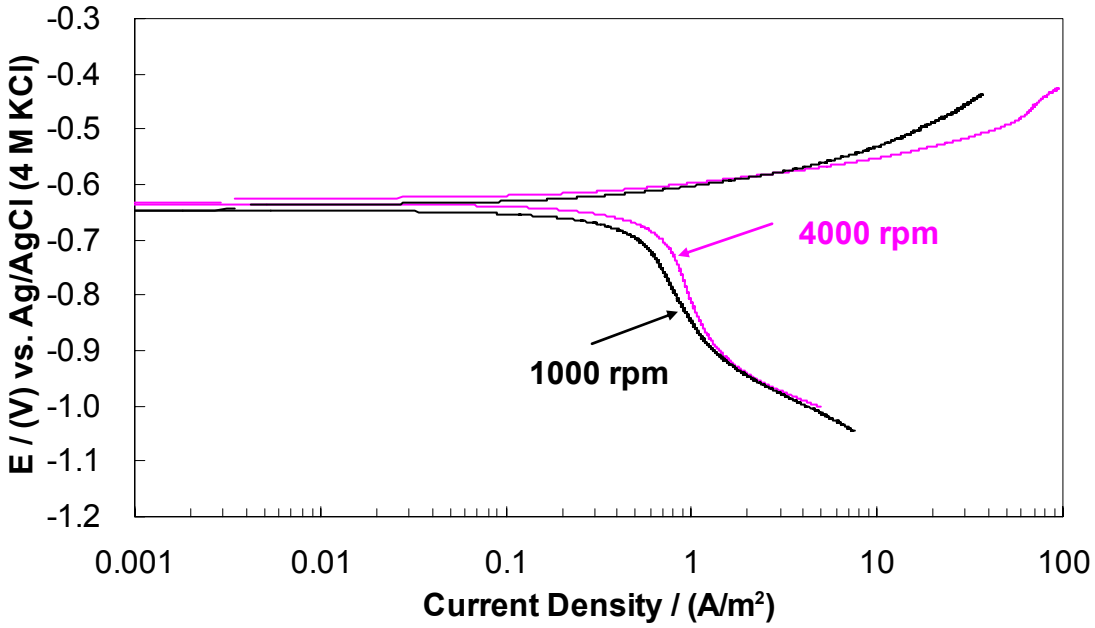

Figure 9. Flow velocity effect on potentiodynamic sweep in CO_2 purged solutions (1000 – 4000 rpm, pH 4, 20 wt% NaCl, 20ºC)

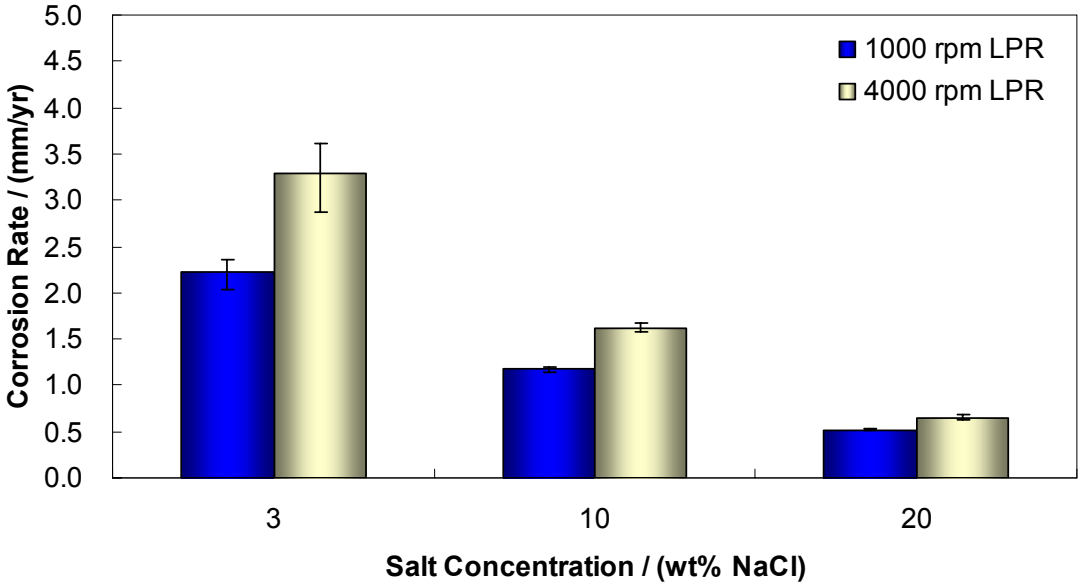

Figure 10. Salt effect on LRP corrosion rate in CO_2 purged solutions (1000, 4000 rpm, pH 4, 3 wt%, 10 wt% and 20 wt% NaCl, 20ºC)

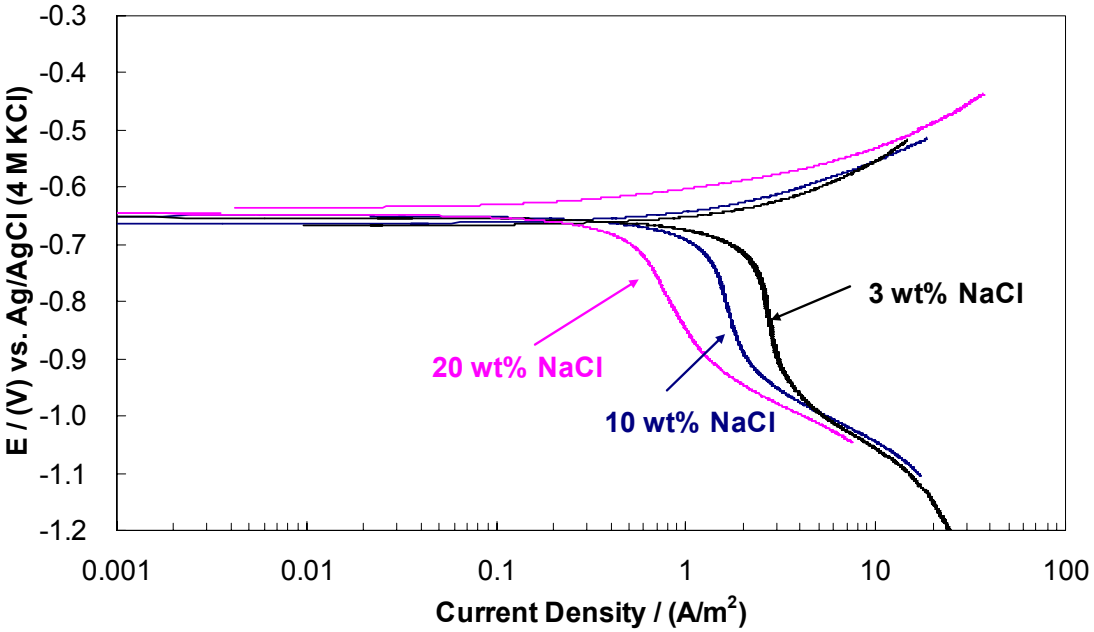

Figure 11. Salt effect on potentiodynamic sweep in CO_2 purged solutions (1000 rpm, pH 4, 3 wt%, 10 wt% and 20 wt% NaCl, 20ºC)

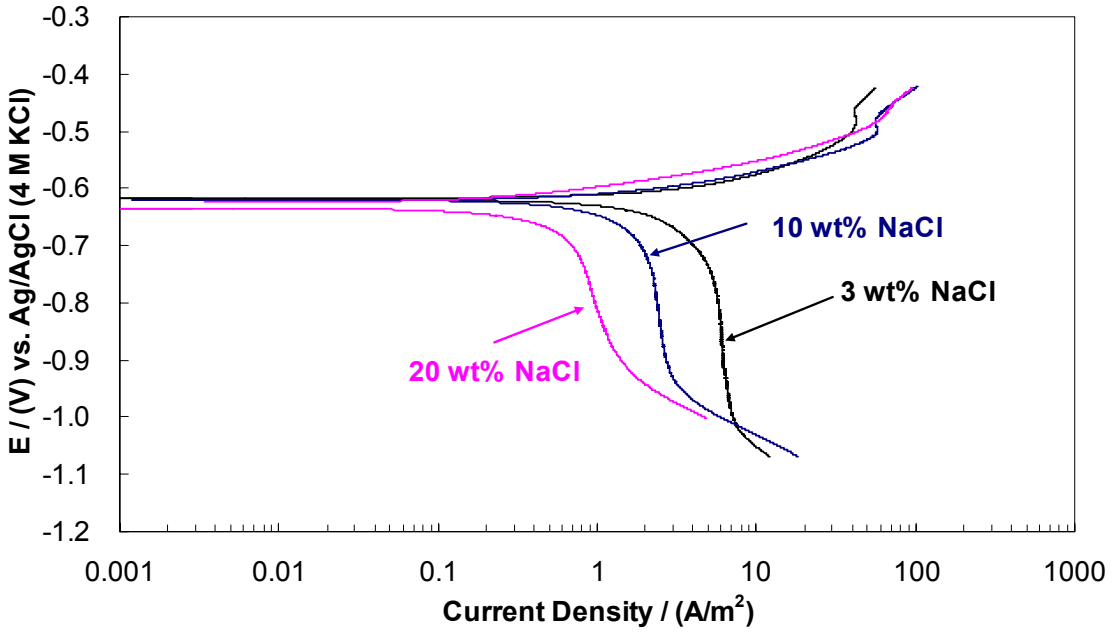

Figure 12. Salt effect on potentiodynamic sweep in CO_2 purged solutions (4000 rpm, pH 4, 3 wt%, 10 wt% and 20 wt% NaCl, 20ºC)

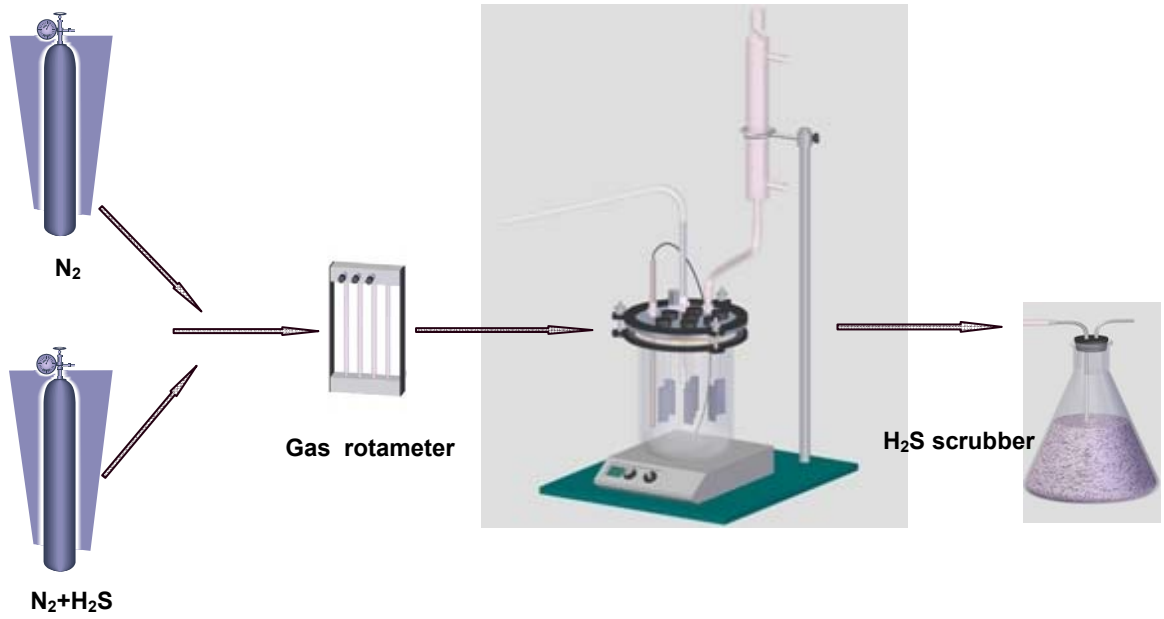

Figure 13. Experimental set-up for H_2S corrosion

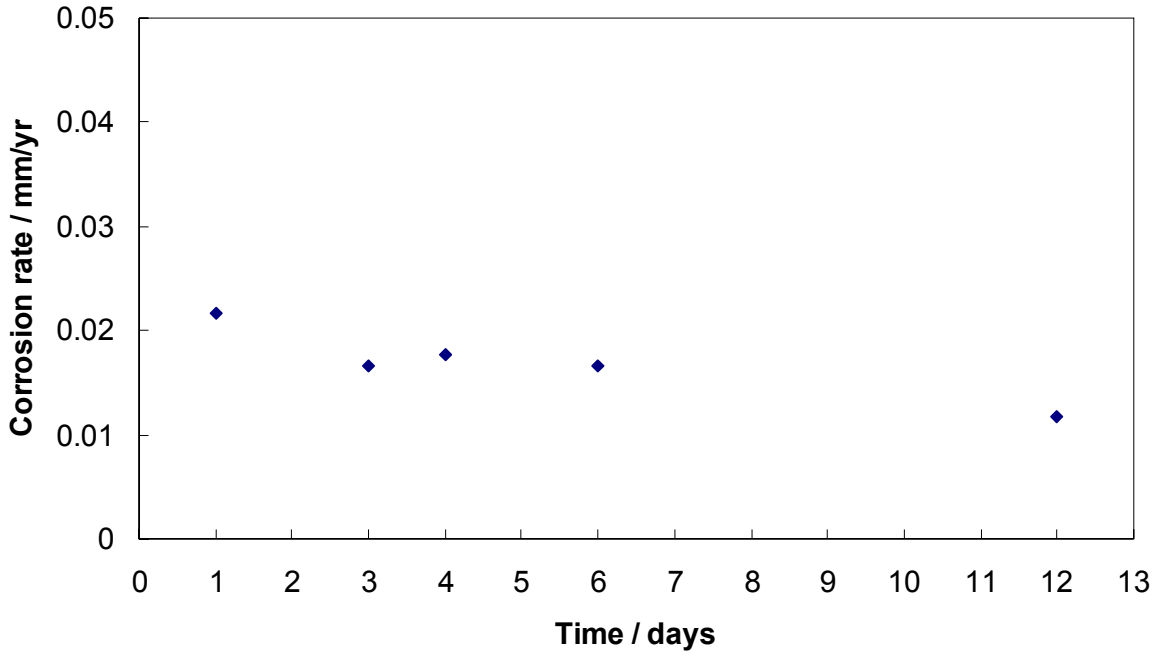

Figure 14. Uniform corrosion rates vs. Time at 25°C, 50ppm H_2S, DI-water.

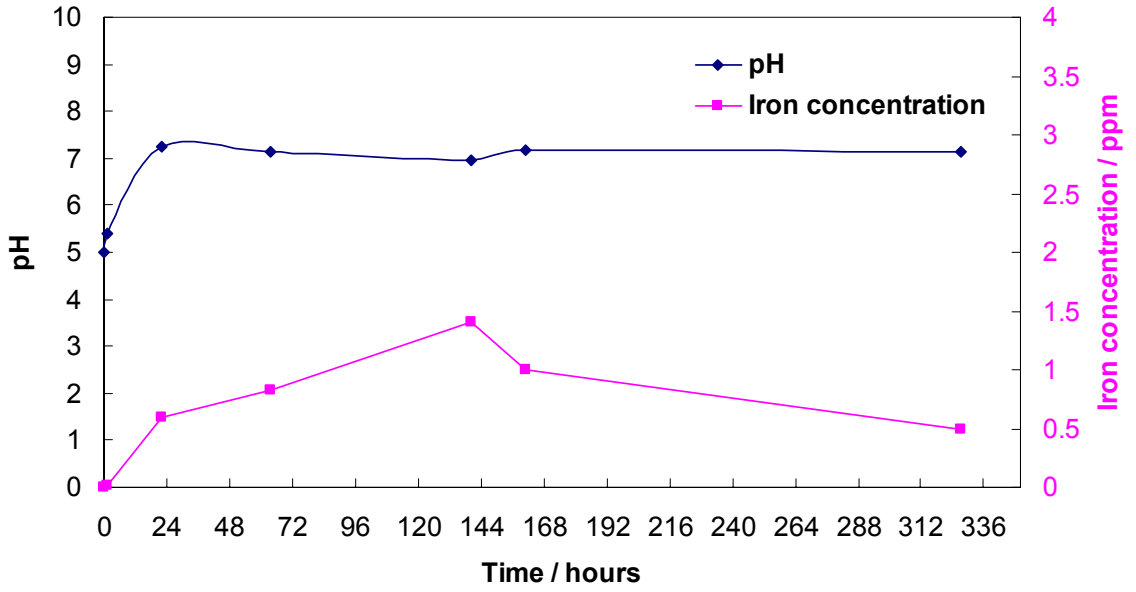

Figure 15. pH and iron concentration change with time at 50ppm H_2S, 0 wt% NaCl, 25°C.

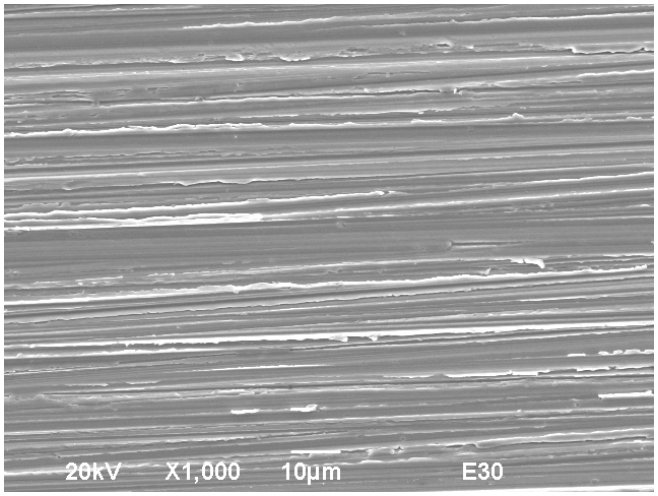

Figure 16. SEM image of bare metal surface polished by sand paper

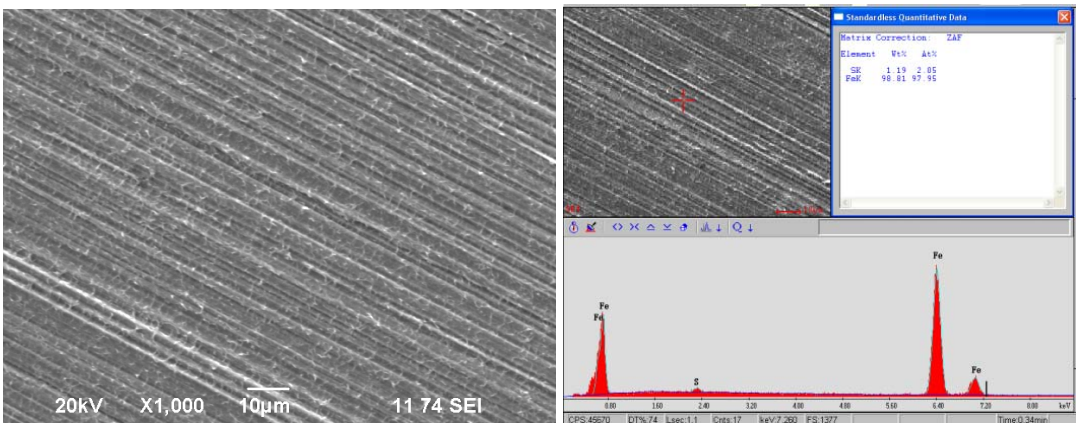

Figure 17. Corrosion specimen exposed to hydrogen sulfide for 1 day at 0 wt% NaCl, 25°C, with film.

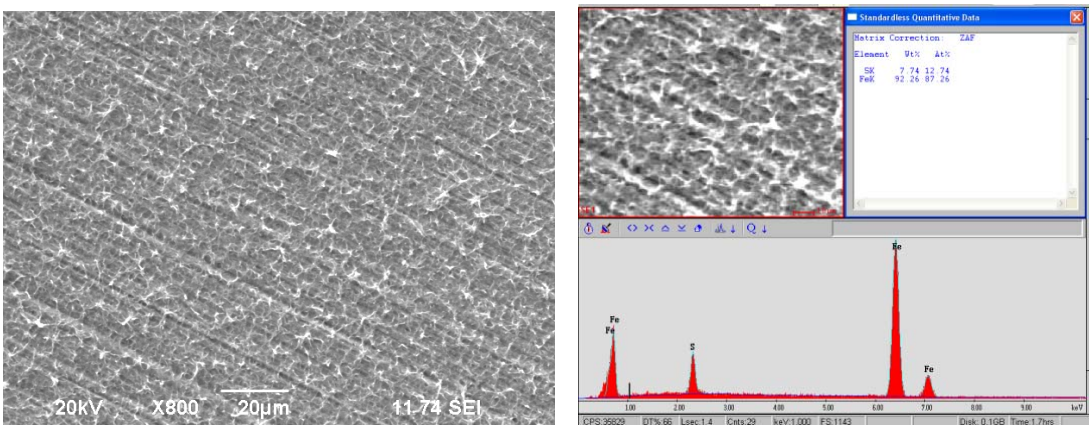

Figure 18. Corrosion specimen exposed to hydrogen sulfide for 4 days at 0 wt% NaCl, 25°C, with film.

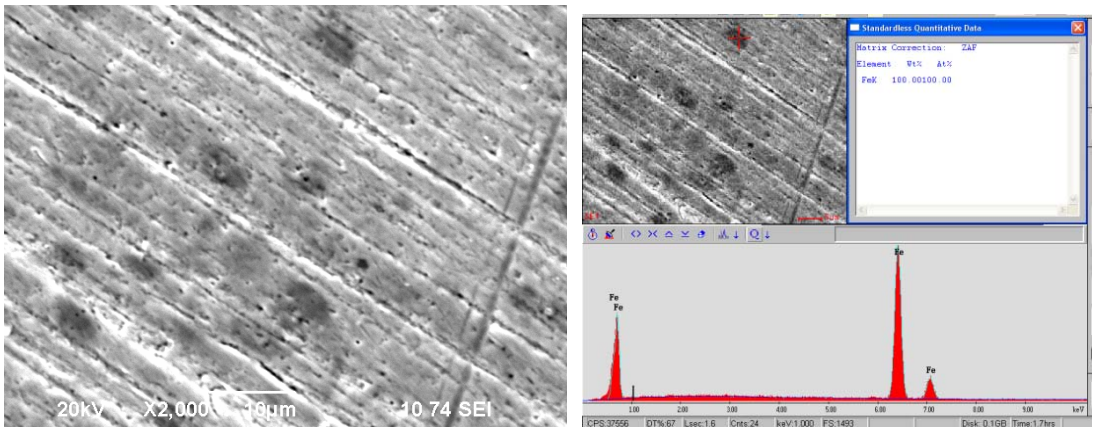

Figure 19. Corrosion specimen exposed to hydrogen sulfide for 4 days at 0 wt% NaCl, 25°C, without film.

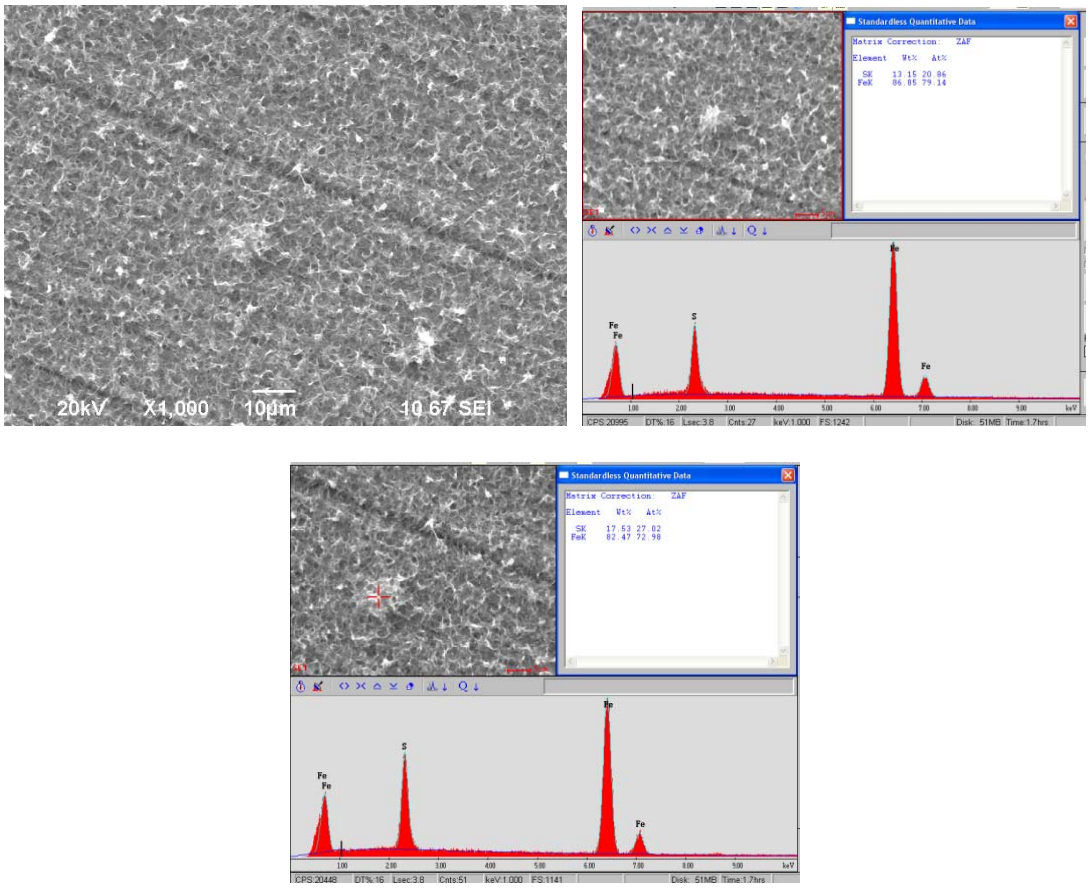

Figure 20. Corrosion specimen exposed to hydrogen sulfide for 6 days at 0 wt% NaCl, 25°C, with film.

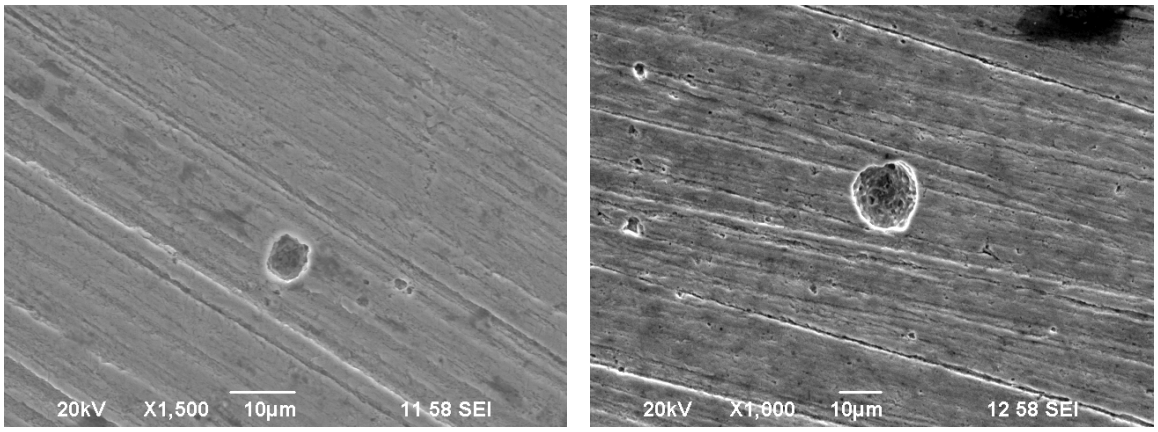

Figure 21. Corrosion specimen exposed to hydrogen sulfide for 6 days at 0 wt% NaCl, 25°C, without film.

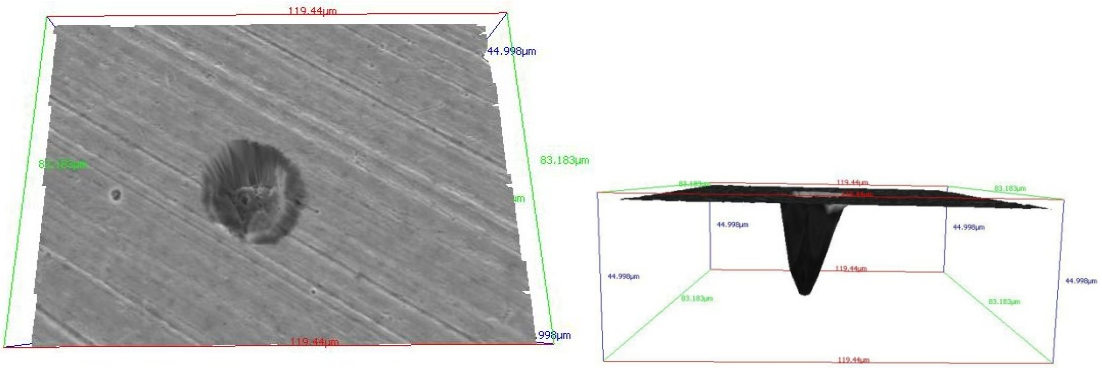

Figure 22. 3D view of corrosion specimen exposed to hydrogen sulfide for 6 days at 0 wt% NaCl, 25°C, without film.

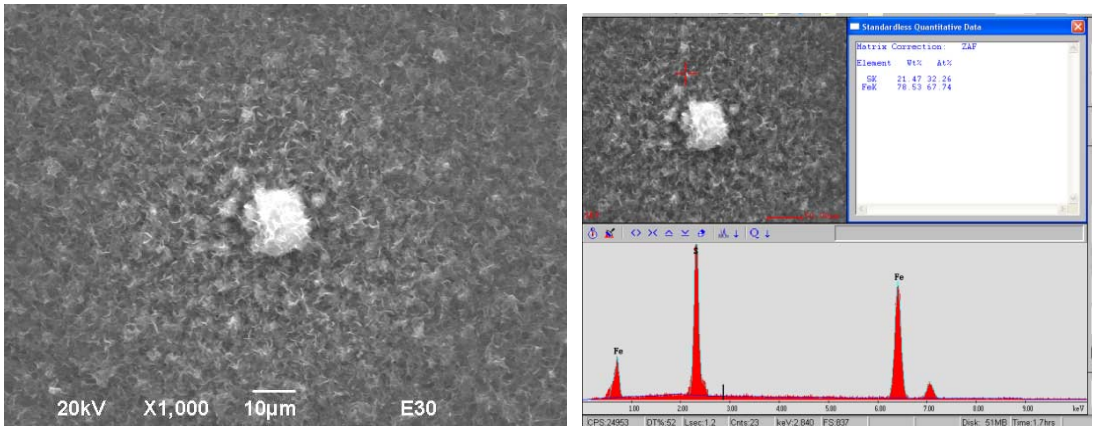

Figure 23. Corrosion specimen exposed to hydrogen sulfide for 12 days at 0 wt% NaCl, 25°C, with film.

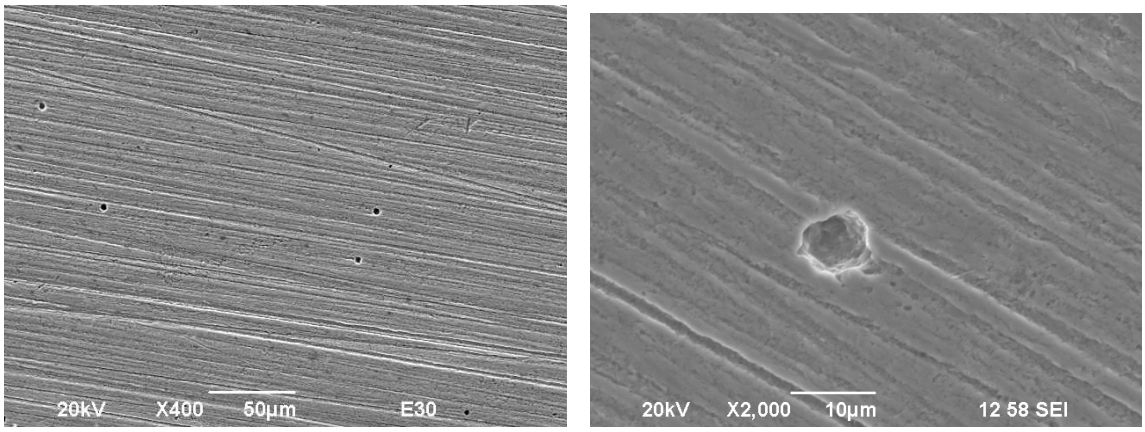

Figure 24. Corrosion specimen exposed to hydrogen sulfide for 12 days at 0 wt% NaCl, 25°C, without film.

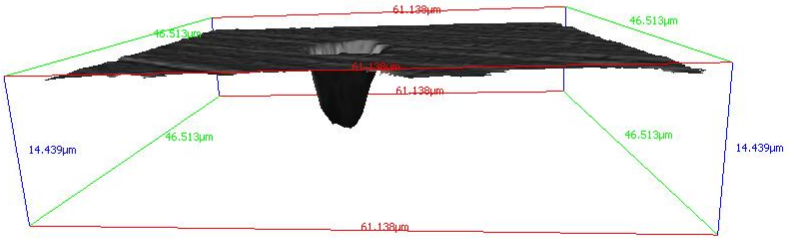

Figure 25. 3D view of corrosion specimen exposed to hydrogen sulfide for 12 days at 0 wt% NaCl, 25°C, without film.

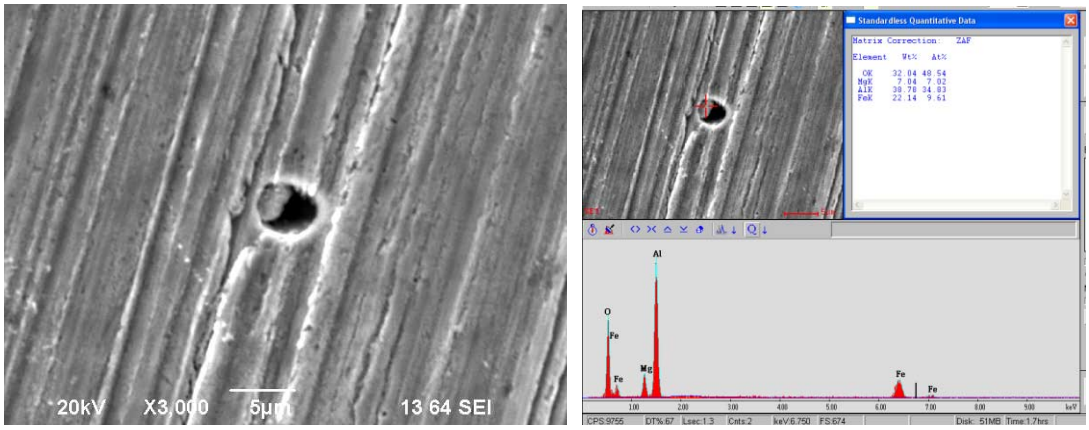

Figure 26. Corrosion specimen exposed to hydrogen sulfide for 6 days at 0 wt% NaCl, 25°C, without film.

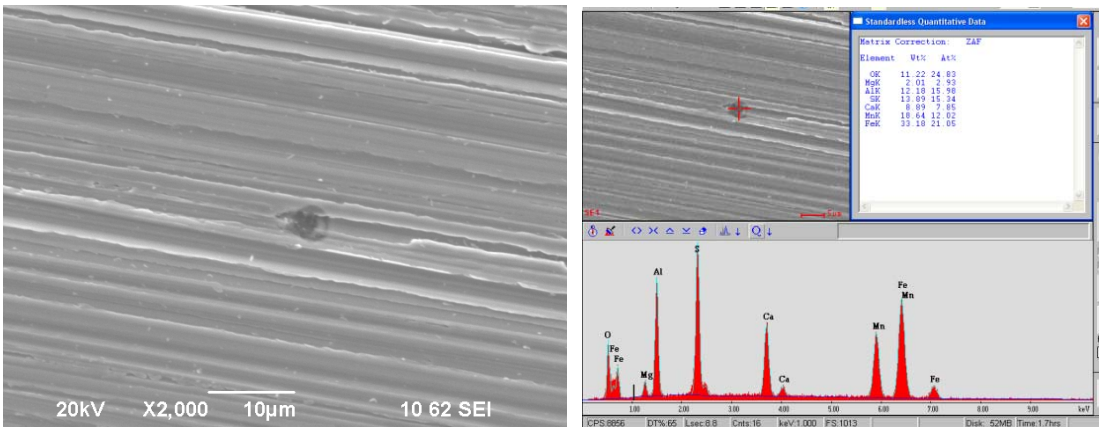

Figure 27. Bare corrosion specimen surface.

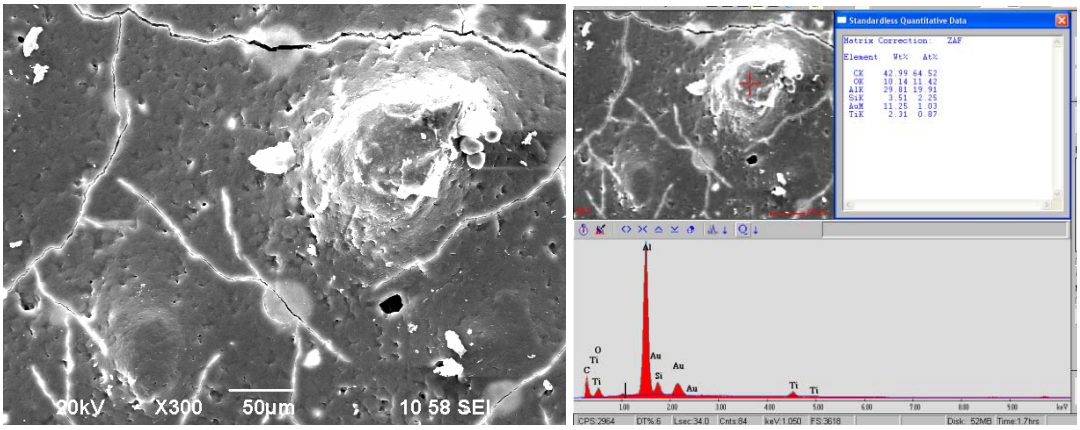

Figure 28. Sand paper covered by gold

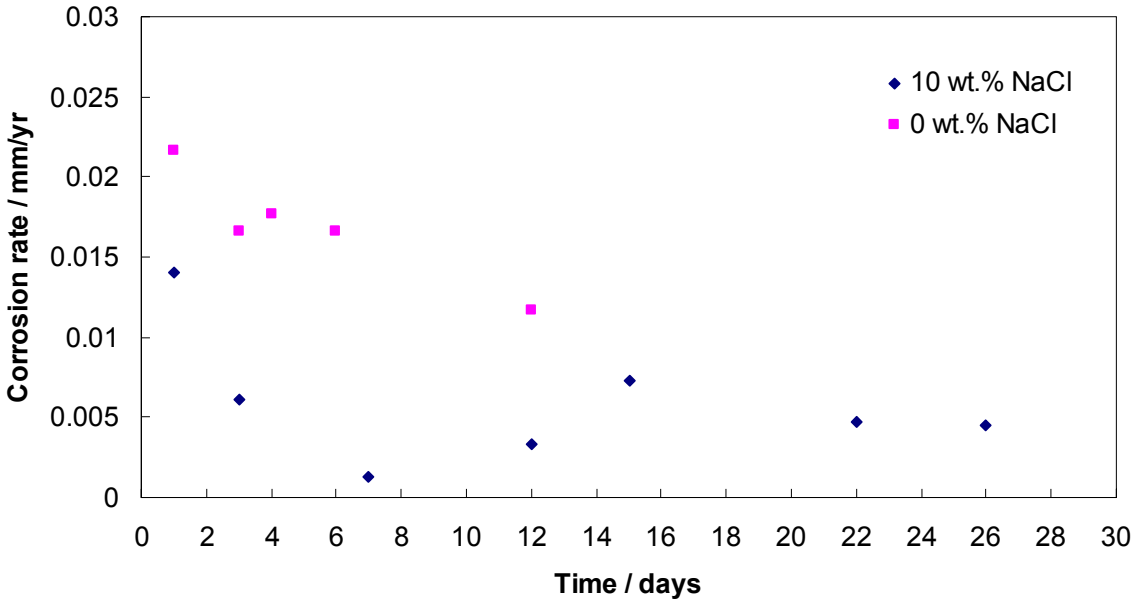

Figure 29. Uniform corrosion rates versus Time at 25°C, 50ppm H_2S, 0 wt% and 10wt %NaCl.

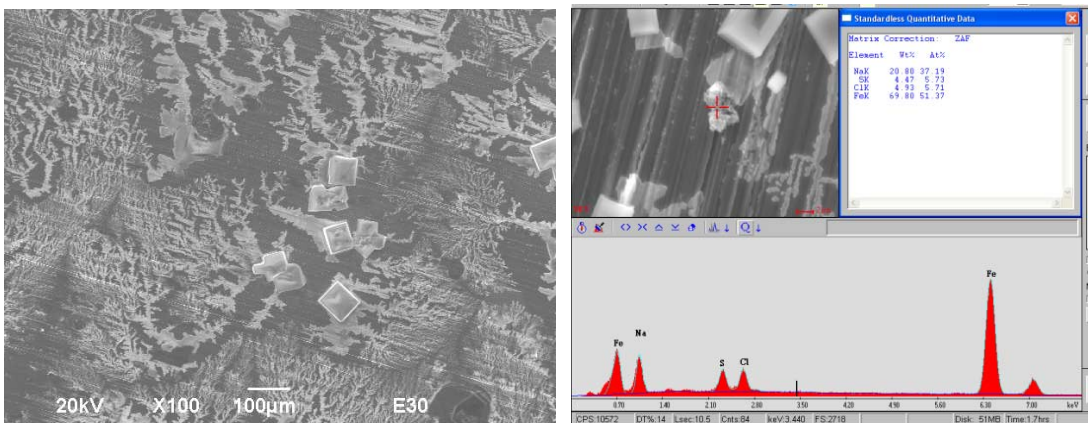

Figure 30. Corrosion specimen exposed to hydrogen sulfide for 1 days at 10 wt% NaCl, 25°C, with film.

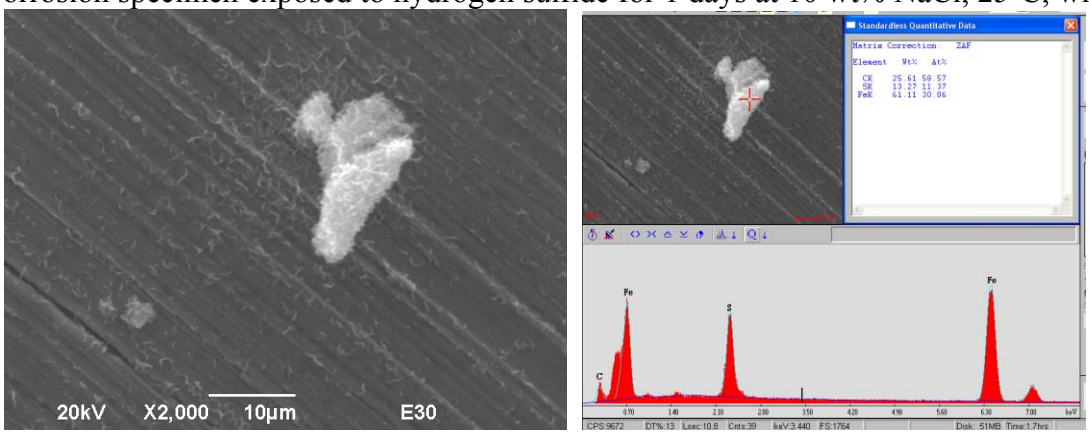

Figure 31. Corrosion specimen exposed to hydrogen sulfide for 3 days at 10 wt% NaCl, 25°C, with film.

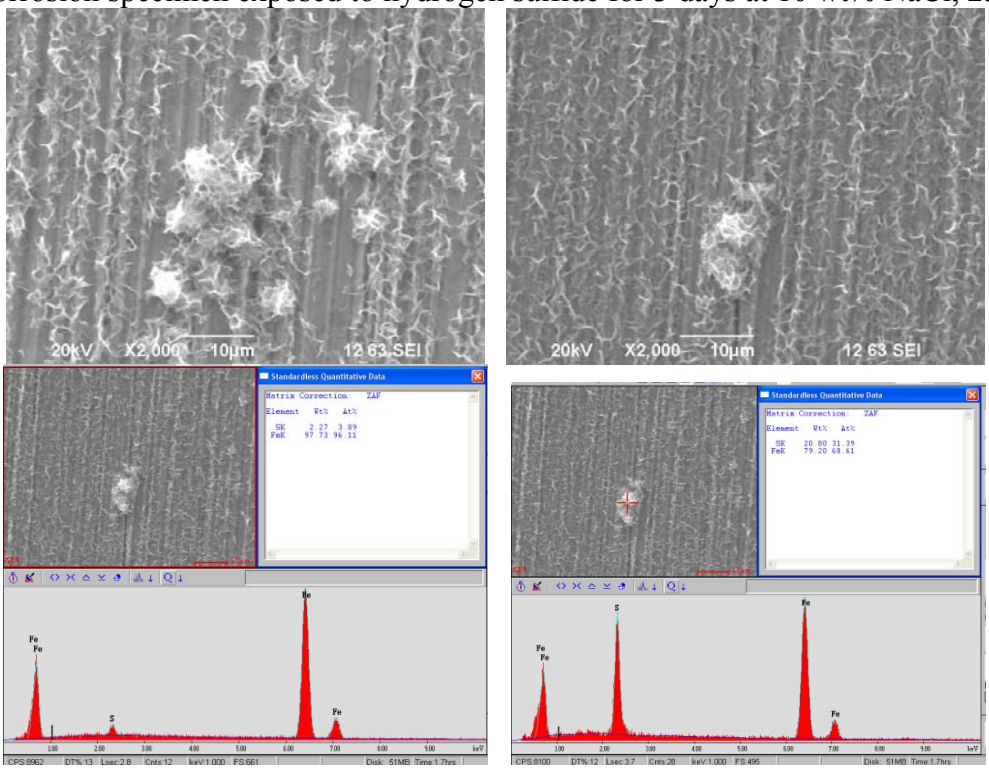

Figure 32. Corrosion specimen exposed to hydrogen sulfide for 7 days at 10 wt% NaCl, 25°C, with film.

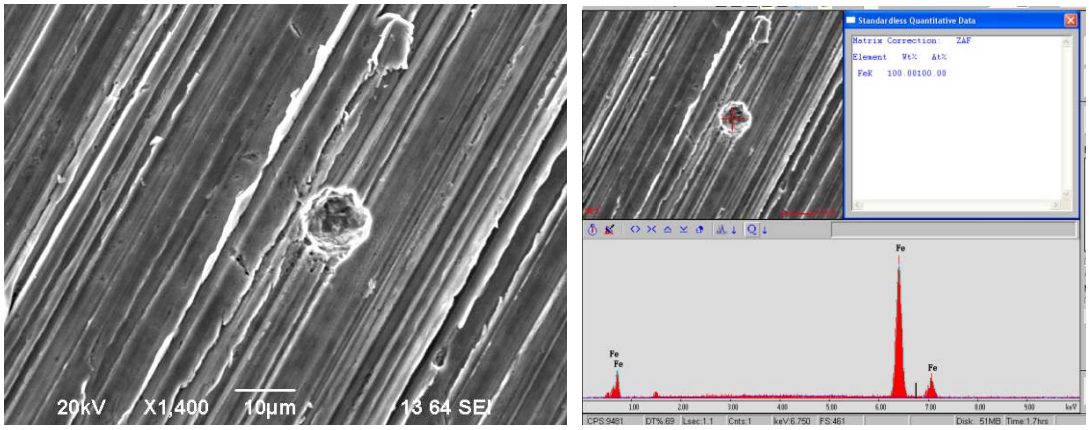

Figure 33. Corrosion specimen exposed to hydrogen sulfide for 7 days at 10 wt% NaCl, 25°C, without film.

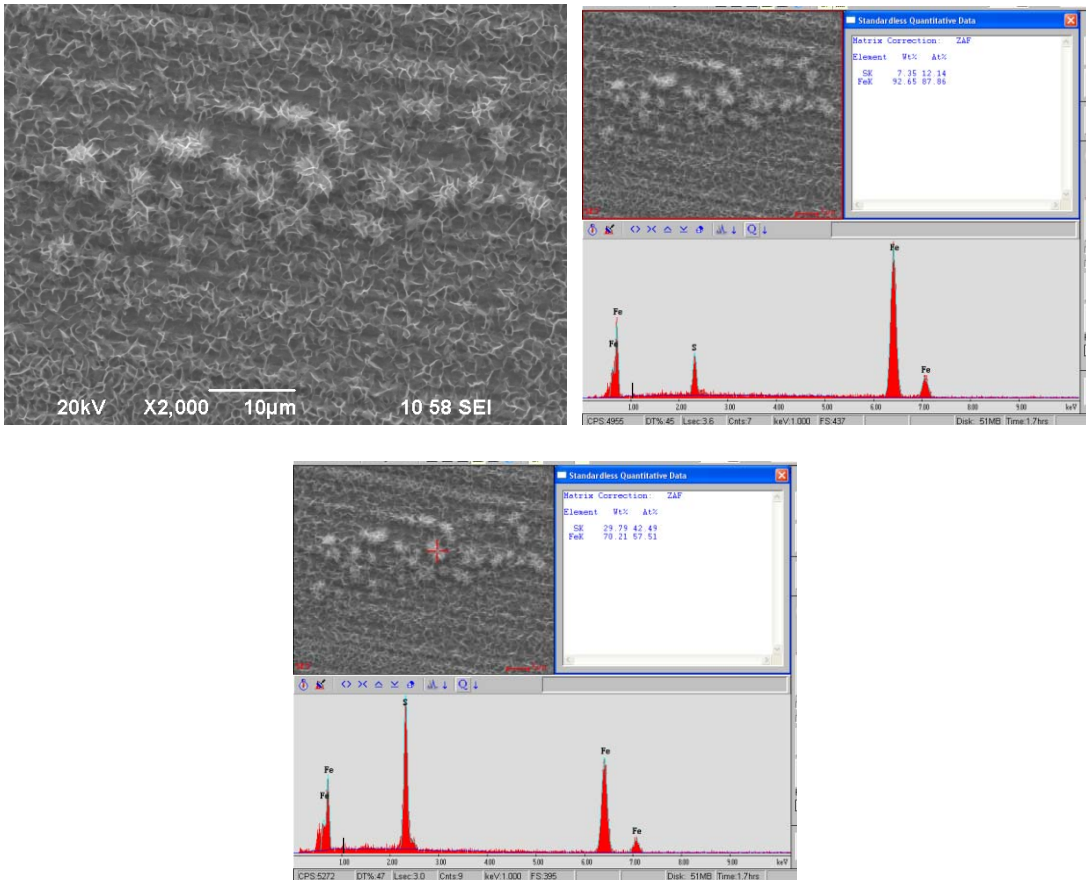

Figure 34. Corrosion specimen exposed to hydrogen sulfide for 15 days at 10 wt% NaCl, 25°C, with film.

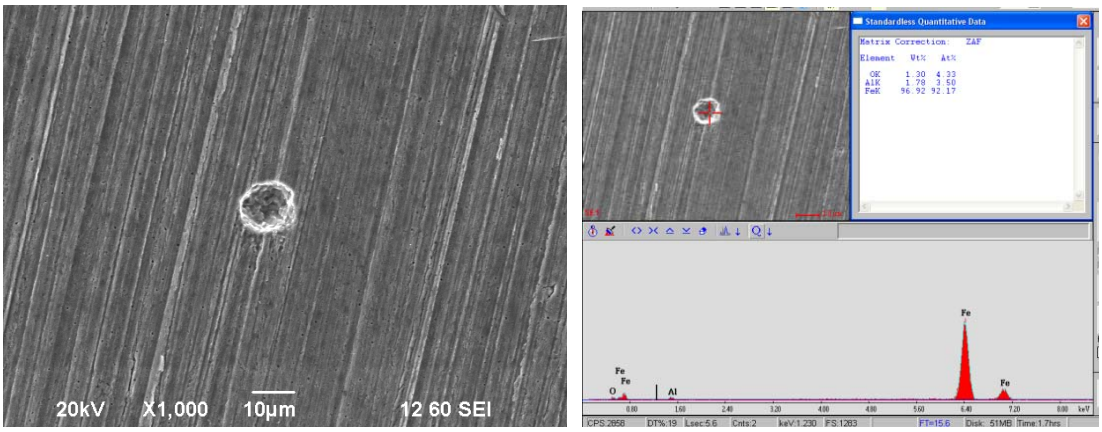

Figure 35. Corrosion specimen exposed to hydrogen sulfide for 15 days at 10 wt% NaCl, 25°C, without film.

Figure 36. 3D view of corrosion specimen exposed to hydrogen sulfide for 12 days at 0 wt% NaCl, 25°C, without film.

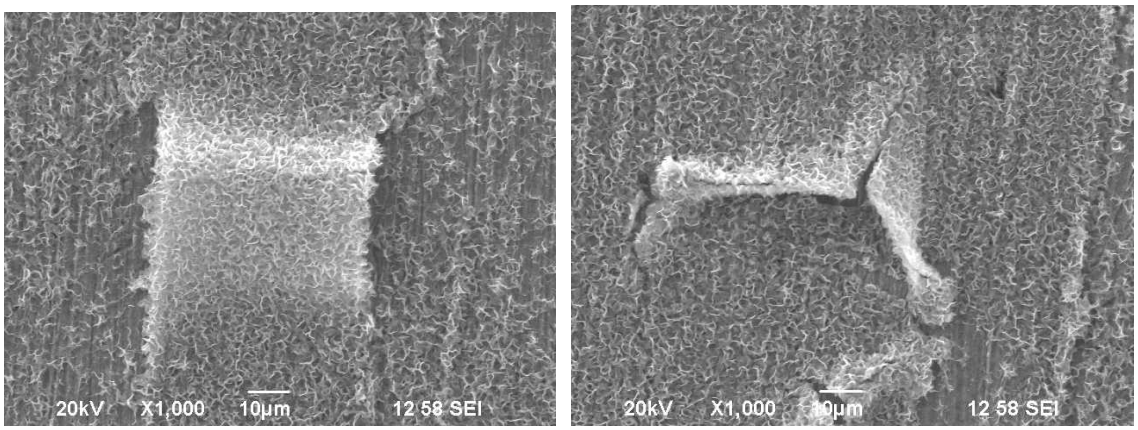

Figure 37. Corrosion specimen exposed to hydrogen sulfide for 26 days at 10 wt% NaCl, 25°C, with film.

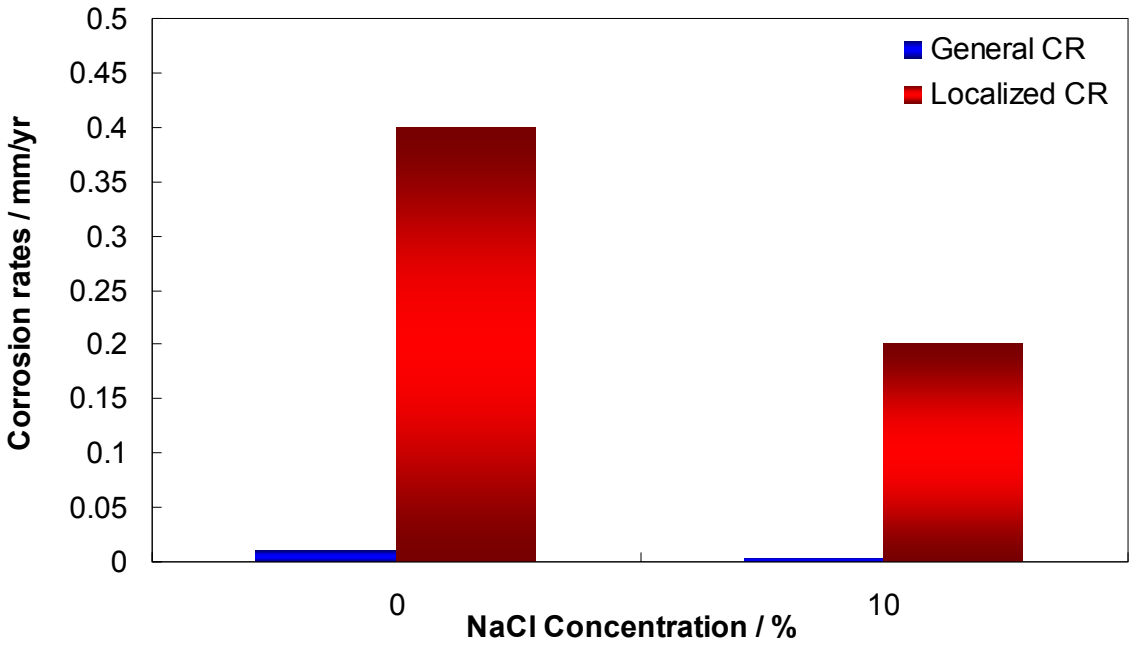

Figure 38. Comparison of localized and general corrosion rate with different salt concentrations at 25°C, 50ppm H_2S, 12 days.